Cement and Concrete Research 133 (2020) 106076

Contents lists available at ScienceDirect

Cement and Concrete Research

journal homepage: www.elsevier.com/locate/cemconres

Structure and morphology of calcium-silicate-hydrates cross-linked with dipodal organosilanes

Amir Moshiri[a], Damian Stefaniuk[a,c], Scott K. Smith[b], Ali Morshedifard[d], Debora Frigi Rodrigues[a], Mohammad Javad Abdolhosseini Qomi[d], Konrad J. Krakowiak[a,*]

[a] Civil and Environmental Engineering Department, Cullen College of Engineering, University of Houston, Engineering Building 1, Room N-107, 4726 Calhoun Road, Houston, TX 77204-4003, United States
[b] Department of Chemistry, University of Houston, TX 77204-4003, United States
[c] Faculty of Civil Engineering, Wroclaw University of Science and Technology, Wybrzeze Wyspianskiego 27, 50-370 Wroclaw, Poland
[d] Advanced Infrastructure Materials for Sustainability Laboratory (AIMS Lab), Department of Civil and Environmental Engineering, Henry Samueli School of Engineering, E4130 Engineering Gateway, University of California, Irvine, CA 92697-2175, United States

ARTICLE INFO

Keywords:
Calcium-silicate-hydrate
Organic-crosslinking
Organosilanes
Structure
Morphology

ABSTRACT

Coupling of organic and inorganic chemistry presents a new degree of freedom in nano-engineering of thermo-mechanical properties of cement-based materials. Despite these vast technological benefits, molecular scale cross-linking of calcium-silicate-hydrate (C-S-H) gel with organic molecules still presents a significant challenge. Herein, we report experimental results on sol-gel synthesis, structure and morphology of nanocrystalline C-S-H cross-linked with dipodal organosilanes. These novel organic-inorganic gels have layered turbostratic molecular structure with similarities to C-S-H precipitating in hydrating cement paste. The organic molecules' chain length controls the interlayer spacing, which shows little to no shrinkage upon dehydration up to 105 °C. However, the structure gets distorted in the basal crystallite plane, in which dimer and trimer Si-polyhedra structures condense on a 2D hexagonal Ca-polyhedra layer. Cross-linked C-S-H gels display plate-like morphology with tendency toward stacking into agglomerates at the larger scale. If successfully realized in cement environment, e.g. high concentration seed, such novel organic-inorganic C-S-H gels could potentially provide cement-based matrices with unique properties unmatched by classical inorganic systems.

1. Introduction

Recent advancements in nanotechnology have opened up new avenues for the “bottom-up” engineering of cement-based materials. This relates not only to more efficient aggregates space filling, a modulation of the pore structure morphology and interfaces at various scales (mesostructure engineering), or tailoring cement hydration kinetics, but also engineering the molecular structure of calcium-silicate-hydrate (C-S-H) gel, the primary binder of concrete [1,2]. In recent years, significant attention has been paid to “inorganic chemistry type approach” and exploration of the effects of calcium-to-silicon (Ca/Si) ratio and atomic substitutions in C-S-H framework on its intrinsic stiffness [3–6], fracture toughness and micro-hardness [7,8], as well as creep [9]. As pointed out by Pellenq et al. [10] and Gmira et al. [11], by changing the nature and bonding scheme of interstitial ions, or the surface charge density of C-S-H nanoparticles one may engineer gel cohesion. Such strategies bear the promise of improving mechanical and physical properties of cement-based materials to some extent; however, to the best of authors' knowledge, it still has limited application and is mostly contained within research laboratories. Moreover, without considerable changes in the type and population of primary bonds existing in C-S-H molecular framework, the impact of such stoichiometric alterations may be very limited to none on certain properties. To illustrate this, consider the example of the intrinsic thermal conductivity of C-S-H. As recently shown by molecular dynamics studies, the stoichiometric modifications, e.g. calcium-to-silicon ratio, appear to be ineffective in the activation of phonon scattering mechanisms, which are imperative for reducing its thermal conductivity at the particle scale [12]. In this case, the deficiency of the “inorganic chemistry approach” is rooted in its inability to reduce the mean free path of phonon in the molecular structure of C-S-H [13].

An alternative approach in the molecular engineering of C-S-H emerges from the coupling of its inorganic framework with organic molecules. If successfully realized in cement environment, and complemented with

* Corresponding author.
E-mail address: kjkrak@uh.edu (K.J. Krakowiak).

https://doi.org/10.1016/j.cemconres.2020.106076
Received 2 October 2019; Received in revised form 15 February 2020; Accepted 6 April 2020
Available online 15 April 2020
0008-8846/ Published by Elsevier Ltd.

optimum design of the mesostructure, such organic-inorganic hybrid C-S-H gels could potentially provide cement-based matrices with unique properties unmatched by the classical inorganic system. For instance, recent investigations on clay minerals [14] show a 5-fold reduction in the thermal conductivity of organoclay nanolaminates compared to unmodified clay. Similarly, incorporating organic cross-linking components into the structure of aerogels reduces material fragility and improves elastic recovery [15]. While the possible technological benefits are vast, still the nanoscale crosslinking of C-S-H with organic molecules is rather considered a research hypothesis to be tested before developing viable technical solutions applicable in hydrating Portland cement systems.

1.1. Polymer intercalation in C-S-H nanocomposites

The problem of synthesis of organic-inorganic (O—I) C-S-H has drawn the attention of various research groups. In particular, the early works of Matsuyama and Young [16–18], which were focused on the synthesis of C-S-H/polymer complexes, showed that the formation of stable hybrid complexes highly depends on the structure of the polymer and C-S-H template stoichiometry. Based primarily on the carbon content and X-ray diffraction measurements they concluded that: a) observed shift in 002 reflection is indicative of organic molecules intercalated in the interlayer space of C-S-H, b) the magnitude of change in the interlayer distance is governed by the type of organic molecule and Ca/Si ratio of the gel, and c) certain type of polymers can be also post-intercalated within already precipitated C-S-H product. For example, for poly(methacrylic acid) (PMA) and poly(acrylic acid) (PAA) polymers, the maximum recorded expansion was about 1.5 nm and 1.2 nm, respectively. The authors suggested, that such large expansion is consistent with the intercalation of ≈2 monomer units in between the layers, and the high amount of polymer content in the complex is unlikely to be explained by the surface adsorption only. However, for small molecular weight polymers such as poly(vinyl alcohol) (PVA) the observed systematic expansion was significantly below the effective diameter of PVA molecule (0.45 nm), and as cautioned in [17] does not present strong evidence of intercalation. Likewise, a small basal expansion in C-S-H / PVA hybrids was also reported by others [19–21]. Based on experimental results, Matsuyama [16,17] hypothesized that the PVA molecule may conform to the ridged surface of the calcium silicate layer resulting in only a slight expansion. Recently, a similar hypothesis was explored by Zhou et al. [22] in studies focused on bulk modulus of C-S-H / PVA nanocomposites. By combining high-pressure X-ray diffraction with molecular dynamics studies, it was demonstrated that the intercalation of PVA molecule within the basal space of C-S-H is feasible, and could explain the decrease in the bulk modulus of O—I C-S-H hybrids relative to regular C-S-H. Moreover, it could also capture an increased degree of silica chain polymerization, which appears to be a common attribute of C-S-H / polymer nanocomposites [17,23–27].

Motivated by the findings reported in [17–19], Merlin et al. [20] looked with additional scrutiny at the problem of possible interactions of C-S-H with various polymers. Following the study of 002 reflection shift measured on O—I C-S-H hybrids synthesized with neutral, anionic, and cationic molecules according to different synthesis methods, including direct precipitation, the experimental evidence pointed toward dominating role of surface adsorption rather than intercalation. Merlin et al. [20] hypothesized, that the high surface charge density of C-S-H layers effectively prevents polymers from entering the interlayer space, thus leaving adsorption as a primary mode of interaction. As a consequence, the texture of C-S-H / polymer hybrids resembles the “meso-composite” [20,28], in which stacked C-S-H lamellae are confined by the surrounding polymer. Moreover, the adsorbed layer of a polymer affects the hydration state of C-S-H particles. Therefore, by retaining more water molecules within the interlayer space some C-S-H / polymer meso-composites may show the expansion of the basal distance as compared to polymer-free C-S-H submitted to the same mild drying. The dominant role of polymer adsorption over intercalation for various types of polymers was also suggested in [25,26,29–31]. For example, while working with hexadecyltrimethylammonium (HDTMA) molecules [25], a dipolar dephasing (DD) ^{13}C CP NMR experiment suggested the location of the methyl groups at the surface of the hydrate rather than incorporated within the layers. However, the possibility of intercalation could not be definitely ruled out either exposing the complexity of assessing interactions between organic molecules and non-stoichiometric solids like C-S-H.

In this respect, testing for possible intercalation in C-S-H still suffers from a certain degree of nonuniqueness of determination. For example, the broadening of 002 basal reflection in C-S-H / polymer nanocomposites has been reported in hybrid gels prepared via direct precipitation [17,20,24,29,30,32,33]. Such broadening might be the effect of a d-spacing distribution in basal direction caused by C-S-H – polymer interactions and/or C-S-H intercalation with variable content of monomers in different conformational states. However, to the best of the authors' knowledge, this particular problem has not been addressed in detail yet, and should be considered in parallel with other phenomena leading to peak broadening, e.g. solid-solution inhomogeneity and crystalline morphology to name just a couple.

1.2. Organosilanes based C-S-H/polymer nanocomposites

The difficulties in overcoming the steric and entropic interactions, which tend to hinder the introduction of the organic molecules within the interlayer of C-S-H, seem to be reduced in sol-gel processing involving functionalized organometallics. In such a processing route, the hydrolysis of alkoxy groups results in numerous silanol bonds (-Si-OH) which condense rapidly to siloxane (-Si-O-Si-) [34], or on the inorganic surface. For example, such a strategy has been successfully applied in the fabrication of layered Al- and Mg- inorganic-organic nanocomposites, with organic functionalities directly linked to the inorganic framework via the Si—C bonds [35]. A similar approach has been used in the pioneering works on organosilane based C-S-H / polymer nanocomposites [36–38]. By studying novel organic-inorganic gels, synthesized via sol-gel method using conventional organosilanes e.g. n-hexyltriethoxysilane (HTES), Minet et al. [36] showed a bi-layer type arrangement of the organic groups inside the interlayer. Moreover, the 002 shift and the length of the alkyl chain are positively correlated, and the molecular structure of such solids may be explained by smectite-type arrangement. However, given the constraint of only one Si—C bond in conventional organosilane, no direct chemical cross-linking in which opposite inorganic galleries are connected via continuous alkyl chain can be realized.

In this work, we explore the idea of direct chemical cross-linking of inorganic galleries of calcium-silicate-hydrates realized through hydrolysis and condensation of functionalized bis-alkoxysilanes (with two Si atoms covalently linked to C atoms at terminal sites of alkyl chain). In particular, the effect of bis-alkoxysilanes on chemistry, structural order, dimensional change upon dehydration, thermal stability, and morphology of stable forms of cross-linked organic-inorganic seeds of calcium-silicate-hydrates are investigated. For this purpose organic-inorganic C-S-H gels were synthesized via sol-gel processing with organosilanes of alkyl [CH_2]-n chain size ranging from 2 to 8, and subjected to scrutinized characterization including, mass spectroscopy (ICP-OES), X-ray powder diffraction, ^{29}Si and ^{19}C NMR, thermogravimetry (TG) and differential scanning calorimetry (DSC), as well as transmission electron microscopy (TEM).

2. Materials and methods

2.1. Sample synthesis

In the synthesis of inorganic and organic C-S-H gels chemical grade, high purity reagents, were used: TEOS (Tetraethyl orthosilicate, 98%, Sigma Aldrich), BTSE (1,2-Bis(triethoxysilyl)ethane, 96%, Sigma Aldrich), 1,6-BIS(Trimethoxysilyl)Hexane (≥95%, Gelest Inc.) abbreviated here as HEX., 1,8-BIS(Triethoxysilyl)Octane (≥95%, Gelest Inc.) abbreviated as OCT., sodium hydroxide (≥97%, Fisher Chemical),

Table 1
Composition of alcohol-based solutions used in the sol-gel synthesis.

Gel type	Solution component					
	Silane (mol)	$CaCl_2$(mol)	HCl(cm^3)	Solvent (cm^3)	NaOH (cm^3)	Ca/Si
TEOS:C-S-H	5×10^{-3}	5×10^{-3}	0.43	11	2	1
BTSE:C-S-H	5×10^{-3}	10×10^{-3}	0.43	11[a]	2	
HEX:C-S-H						
OCT:C-S-H						

[a] Ethyl alcohol used in the synthesis of TEOS:C-S-H, BTSE:C-S-H and OCT:C-S-H, methyl alcohol used in the HEX:C-S-H synthesis.

calcium hydroxide (≥96%, Fluka®, Honeywell), calcium chloride (≥93%, Sigma Aldrich), 0.1 M hydrochloric acid (Titripur®, Merck KGaA), ethyl alcohol (200 proof, Decon Labs. Inc.), methyl alcohol (anhydrous, Macron Chemicals), distilled ASTM Type II water (Aqua Solutions Inc.). To avoid possible carbonation of gels the synthesis was performed inside the glove box in the N_2 atmosphere with continuously monitored CO_2 concentration.

At the sol-gel processing stage, organo-silane reagents were hydrolyzed at room temperature in the alcohol-based solution of HCl and $CaCl_2$ (see Table 1). Hydrolysis was performed under continuous steering for 8 h. Next, 19 M NaOH solution was rapidly added and homogenized for an additional 12 h. Injection of NaOH solution resulted in pH shift to highly basic conditions and gel formation. Precipitated gels were centrifuged and washed 4 times in the preconditioned aqueous solution doped with 2×10^{-3} M $Ca(OH)_2$. Such dosage corresponds to [Ca] = 2 mM, which represents Ca equilibrium concentration with C-S-H solid of Ca/Si ratio 1 preventing possible decalcification [39]. Finally, all gels were vacuum dried at 50 °C for 24 h, above the silica gel, and stored in sealed vials prior to characterization work.

2.2. X-ray powder diffraction

Powder diffraction patterns were collected with a PANalytical X'Pert PRO XRPD multipurpose diffractometer configured in Bragg-Brentano geometry, with a high-speed, high-resolution X'Celerator position sensitive detector, a Cu – anode source (Cu K-alpha $\lambda = 1.541$ Å) operating at 45 kV and 30 mA, 10 mm mask and 0.5° antiscatter slit. Two types of scans were carried out: a) high resolution scan in the 2θ range 3 to 15° targeting the basal spacing reflection, and b) broad scan from 5 to 60° to obtain global diffraction pattern. All scans were run at a step size of 0.017° and a speed of 360 s./step and 88.3 s./step in high resolution and broad scans, respectively. Experimental X-ray patterns were analyzed in HighScore Plus® (PANalytical) package and compared to Powder Diffraction Files (PDF) from the database published by the International Centre for Diffraction Data (ICDD).

2.3. Chemical analysis

Inductively coupled plasma optical emission spectroscopy (ICP-OES) was used for elemental analysis of synthesized gels (Agilent 725 ICP-OES, Agilent). For this purpose, representative samples for ICP-OES were prepared via flux-fusion method [40]. This includes the preparation of glass beads from 0.1 g of calcium-silicate-hydrate gel mixed with 0.5 g of $LiBO_2$ flux and 100 μL of LiBr wetting agent fused in carbon crucible at 1050 °C for 20 min. After cooling, the fused disk was transferred to Teflon bicker and dissolved in 25 mL of 1 M HNO_3 under continuous stirring. The resulting fluid was filtered and additionally diluted with 25 mL of nitric acid. The final analyte solution was prepared by sampling 1 g of the filtered solution and diluting with 9 g of 1 M HNO_3. All analyte solutions were analyzed for elemental concentrations of Ca, Si and Na.

2.4. ^{29}Si MAS NMR and ^{13}C CP-MAS NMR

Nuclear Magnetic Resonance (NMR) spectra were collected at room temperature with JEOL ECA500 NMR (JEOL, Japan) spectrometer equipped with 11.74 T magnet operating at 99.33 MHz for ^{29}Si and 125.73 MHz for ^{13}C, respectively. Samples were packed in 3.2 mm rotors (zirconia with vespel endcaps). ^{29}Si data were collected at 15–18.5 kHz MAS spin rate; averaged over 360 scans of 1024 complex points with 90 degree pulse (7 us) and 180 s between acquisitions to achieve quantitative results. Sweep width was 300 ppm centered at −100 ppm, with TPPM ^1H decoupling (nominal pulse width 2.8 μs for 90 deg). ^{13}C data were collected at 12.5 kHz MAS spin rate, under CP-MAS conditions: 1024 scans of 2048 complex data points were collected over 400 ppm ranges and centered at 50 ppm. CP power levels were calibrated for 10 ms starting with ~3 us 90° pulse widths for both ^1H and ^{13}C on a sample of adamantane spinning at 12.5 kHz. TPPM ^1H decoupling at nominal 2.8 μs (90 deg) pulse and relaxation delay 5 s was applied. Acquired NMR data were processed and analyzed with JEOL Delta v5.3 package. Processing of time domain data included exponential multiplication (150 Hz for Si and 20 Hz for C), 2× zero filling, Fourier transform (FT), manual phase adjustment and baseline correction. Relative integral intensities were obtained from decomposition with mixed Lorentzian-Gaussian peak profile.

2.5. Thermogravimetric and calorimetry analysis (TG/DTA, DSC)

Thermogravimetric analysis (TG) was performed on all dried powders. All experiments were carried out in Discovery TGA 550 Advanced (TA Instruments) at the temperature rate 20 °C/min up to a maximum temperature of 980 °C and under the N_2 atmosphere. Minimum 3 samples for each gel type were tested with the average sample weight around 20 mg inside the Pt TGA pan. Additionally, all C-S-H gels were examined in differential scanning calorimetry (DSC), DSC 1 System (METTLER TOLDEO). For DSC experiments, samples were heated from 25 °C to 700 °C at the rate of 20 °C/min under the N_2 atmosphere.

2.6. Transmission electron microscopy (TEM)

The particle morphology and crystallinity of selected gels were investigated in the transmission electron microscope (JEOL 2010F). For sample preparation, the previously dried gel was dispersed in pure ethanol using ultrasonicator for 4 min and then a drop suspension was deposited on a lacy carbon film. High-resolution (HR) TEM micrographs were taken with an electron beam operated at 200 kV.

3. Experimental results and interpretation

The sol-gel processing provides a unique opportunity for manipulation of the molecular structure of C-S-H with organometallic molecules. The effects of such modification on the long-range order, solid stoichiometry, as well as physical and thermal properties are presented next.

3.1. ICP-OES gel stoichiometry

Measured concentrations of major elements (except carbon, C) constituting synthetic C-S-H and its organic hybrids are reported in Table 2. In most cases, Ca/Si atomic ratio of the precipitate is close to 1, which is the initial molar ratio of alcohol-based solutions used in organosilane hydrolysis. The observed discrepancy is attributable to the ICP-OES measurement uncertainty. However, in the case of HEX:C-S-H gel the Ca/Si molar ratio is slightly below the target value designed in the experiment suggesting close to but not optimum synthesis conditions have been achieved. Finally, the highest uptake of alkaline ion Na^+ is recorded for reference C-S-H gel, around 1%, while in hybrid gels it is significantly lower.

Table 2
Chemical composition of synthesized gels as measured with ICP-OES.

Gel Type	Element[a]					
	Ca (wt%)	Si (wt%)	Na (wt%)	Ca (mol)	Si (mol)	Ca/Si[b]
TEOS:C-S-H	24.17 ± 1.07	16.65 ± 0.91	1.16 ± 0.15	0.60 ± 0.03	0.59 ± 0.03	1.02 ± 0.03
BTSE:C-S-H	22.95 ± 0.16	16.13 ± 0.42	0.32 ± 0.15	0.57 ± 0.01	0.57 ± 1.01	1.00 ± 0.03
HEX:C-S-H	18.72 ± 1.48	13.92 ± 1.02	0.09 ± 0.02	0.47 ± 0.04	0.50 ± 0.04	0.94 ± 0.08
OCT:C-S-H	15.90 ± 0.72	10.85 ± 0.24	0.27 ± 0.01	0.40 ± 0.02	0.39 ± 0.01	1.03 ± 0.02

[a] Average of three measurements, error values correspond to one standard deviation.
[b] The estimated max. relative standard deviation (RSD) on Ca/Si due to analytical precision, obtained on replicated analysis of controlled gel specimens is 4%.

3.2. X-ray powder diffraction

The first direct evidence of successful incorporation of organometallic molecules into the molecular structure of synthesized gel is provided by X-ray powder diffraction performed in the low 2θ range (Fig. 1), which encompasses the basal reflection d_{002} of C-S-H [41]. It is observed that incorporation of longer $[CH_2]_n$ chains (BIS) organosilanes increases the interlayer spacing relative to TEOS: C-S-H d_{002} reflection located at ≈12.7 Å (≈7° 2θ). This effect is especially evident for organosilanes with chain length $n = 6$ (HEX: C-S-H) and $n = 8$ (OCT: C-S-H). Thus, a stratified molecular structure with long-range order in the **c**-direction has been established with possible condensation of silica tetrahedron on the Ca polyhedron layers. A similar trend in the expansion on the unit cell was reported by Minet et al. [36] for organosilicate hybrids incorporating silanes with only one Si−C bond and non-hydrolyzable organic moiety, e.g. n-hexyltriethoxysilane (HTES). On the contrary, the basal reflection position in BTSE modified C-S-H remains unchanged relative to TEOS:C-S-H, suggesting that small size organic molecules can be accommodated within the interlayer space without causing dilation along **c** crystal axis. In addition, such small molecules seem to lead to a lower degree of crystallinity and/or crystallite size as indicated by the largest broadening of the basal peak. The estimated value of FWHM for basal reflection (d_{001} in modified gels [35,36]) in BTSE:C-S-H sample is around 30% and 50% greater than in gels synthesized with molecules of alkyl chain size 6 (HEX:C-S-H) and 8 (OCT:C-S-H), respectively. It must be mentioned, the X-ray spectra of all hybrid gels were collected under the same analytical conditions, and therefore it may be assumed that the instrument broadening has a similar contribution to FWHM estimates.

The change in the interlayer distance upon continuous dehydration is another important point worth consideration here. One of the commonly used mineral analogs, based on which the C-S-H structural models are proposed, is 14 Å tobermorite [41–43]. By heating tobermorite, a reduction in the interlayer distance is obtained through the progressive dehydration process [44,45]. Likewise, the basal spacing of quasi-crystalline C-S-H shrinks upon losing the interlayer water [46]. For C-S-H with $CaO/SiO_2 \approx 1$, the contraction from ≈13 Å (mild drying conditions) to ≈11 Å (harsh drying) has been reported [42,43,47]. Similar behavior is observed in the baseline TEOS:C-S-H sample (Fig. 2), where the contraction of d_{002} from 12.6 Å (≈7°2θ) to 10.8 Å (≈8°2θ) is recorded upon changing drying conditions from 50 °C to 105 °C. However, a very contrasting phenomenon is displayed by organic-inorganic C-S-H hybrids. As revealed by X-ray data (Fig. 2), the interlayer spacing in these materials is not affected by changing the drying conditions from mild to more severe, indicating no shrinkage along **c**-direction. Such retention of the basal distance can be realized by the cross-linking of Ca-galleries with alkyl chains, thus providing another experimental evidence of the successful hybridization of calcium-silicate-hydrate. It must be noted, the possibility of organosilane molecules present in the different conformational states within the interlayer space cannot be excluded at the current stage and requires further investigation.

The incorporation of the organic molecules within the molecular framework of C-S-H hybrids has also important implications for the structural order in **a-b** plane. Accordingly, as presented in Fig. 3a the reference TEOS:C-S-H sample exhibits a few and broad diffraction maxima located at 5.34 Å, 3.04 Å, 2.81 Å, 2.06 Å, 1.83 Å, and 1.67 Å, many of which are *hk0* type. This is in line with the commonly observed set of reflections systematically observed in patterns from synthetic and OPC based C-S-H [39,42,43,48,49]. Of particular importance is the

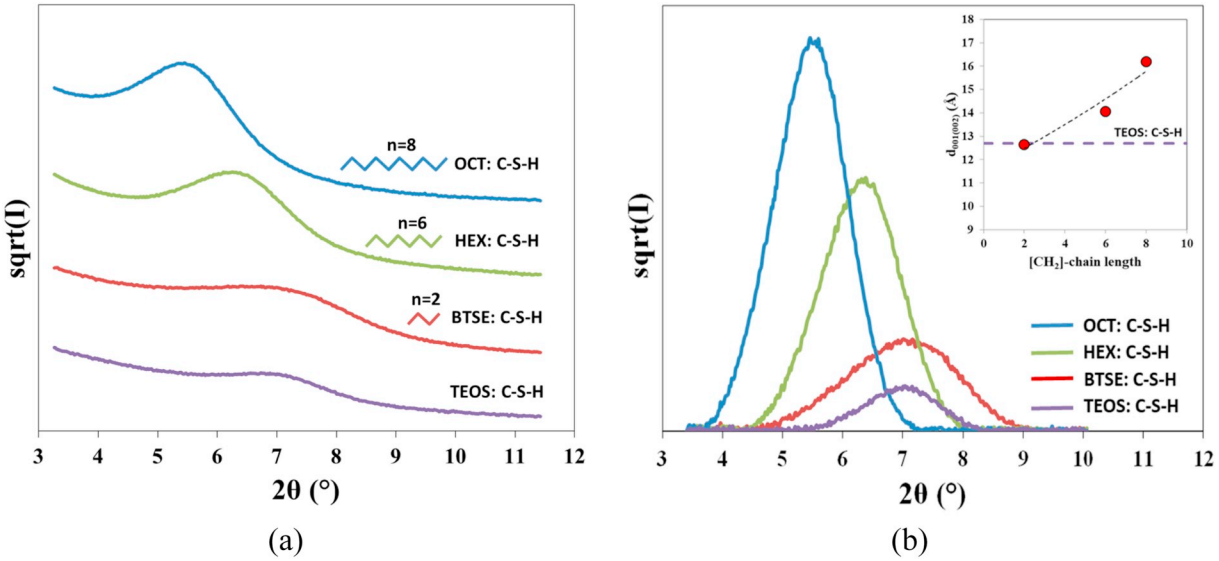

Fig. 1. Basal reflection position in the C-S-H gels modified with BIS-organosilane molecules: (a) raw X-ray diffraction spectra, (b) basal diffraction peaks isolated after background removal, change in basal distance vs. $[CH_2]$ – chain length presented on the inset. Powders dried for 24 h at 50 °C under vacuum.

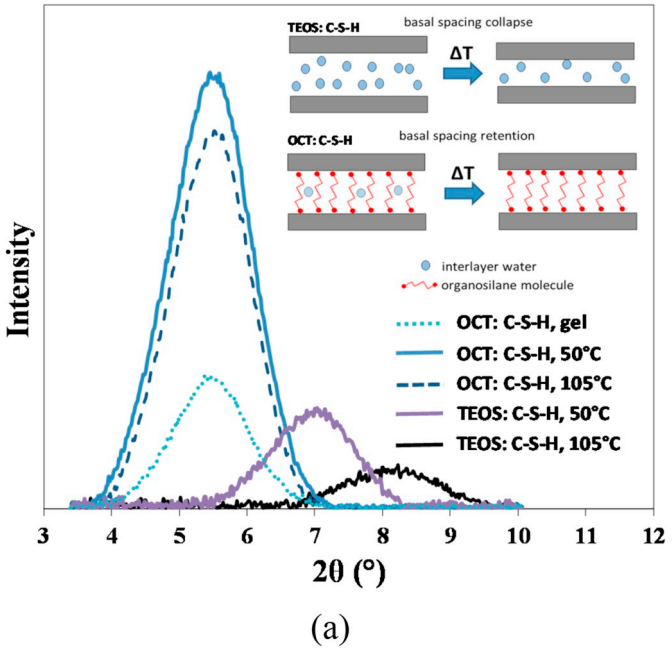

Fig. 2. Effect of dehydration on the interlayer distance in the TEOS: C-S-H and calcium silicate hydrates modified with bridged bipodal (BIS)-organosilanes OCT: C-S-H.

triplet {3.04 Å, 2.81 Å, 1.83 Å}, which corresponds to coherent scattering from regularly arranged atomic planes, e.g. calcium in the polyhedral calcium layer (Fig. 3b).

A quite different picture is obtained on the hybrids of C-S-H gel synthesized with organosilanes. The main differences include: (a) reduced number of diffraction events corresponding to coherent X-ray scattering in **a-b** plane, (b) increased broadening in which maxima tend to take the form of wide bands, and (c) clear asymmetry of the main band centered at ≈30°deg. 2θ angle. BTSE, HEX and OCT: C-S-H gels show a common pattern with the broad bands located at ≈3.05 Å and ≈1.8 Å. However, the band located at ≈4.5 Å is missing in the BTSE: C-S-H, which was synthesized using the shortest carbon chain organosilane, $n = 2$. Based on these results, it is apparent that the molecular structure of hybrid C-S-H gels shows a lower degree of ordering in **a**-**b** plane as compared to their inorganic counterpart TEOS: C-S-H.

Given the XRD observations, it is worth asking whether some conclusions can be reached regarding the possible stratification of the Ca atoms within the central layer of C-S-H hybrids. By analogy to tobermorite, C-S-H comprises of "stratified" calcium polyhedra, which are displaced along **c** axis by ≈2 Å relative to each other (Fig. 4a). Depending on the crystal variety, the unit cell has an orthorhombic or monoclinic character. On the contrary, the Ca atoms in portlandite structure form planar sheaths (see Figs. 3c and 4b) and the unit cell is hexagonal [43]. A typical feature of the hexagonal unit cell is the ratio d_{100}/d_{110}, which has theoretical value $\sqrt{3} \approx 1.732$. If the two main reflections observed in the hybrid gels are assigned to 100 and 110 planes, respectively, their *d*-spacing ratio is around 1.704 for OCT: and HEX: C-S-H gels, which is close to the theoretical value. However, in BTSE: C-S-H gel this ratio is significantly lower, 1.687. This observation, together with observed trends in the basal reflection (Fig. 1b), suggests the nanocrystalline turbostratic structure of hybrid gels in which randomly stacked hexagonal layers of Ca-polyhedra display systematic random translations or/and rotations between adjacent sheets [50].

The in-plane hexagonal symmetry and turbostratism of (Al, Mg, Ca)-alkylsilicates, derived from the sol-gel processing of trialkoxysilane with n-alkyl functionality, has been also suggested by Ukrainczyk et al. [35] and Minet et al. [36]. By using the analogy with 2:1 trioctahedral Mg-phyllosilicates, e.g. smectite, the latter authors estimated a Ca−Ca distance of 0.351 ± 0.005 nm, which is close to the $d_{Ca\text{-}Ca}$ found in the brucite-like layers of portlandite.

3.3. ^{29}Si MAS NMR and ^{13}C CP-MAS NMR

The insight into the chemical environment of silicon contained in the structure of reference C-S-H, as well as its hybrids with organic

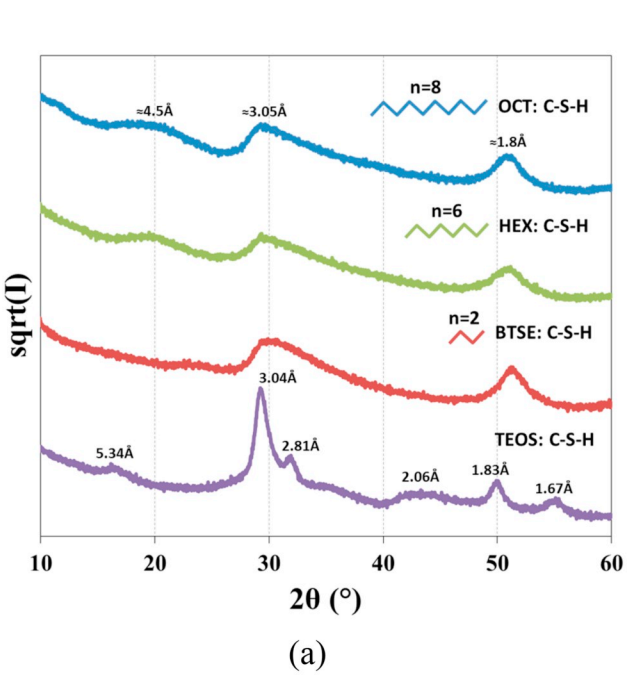

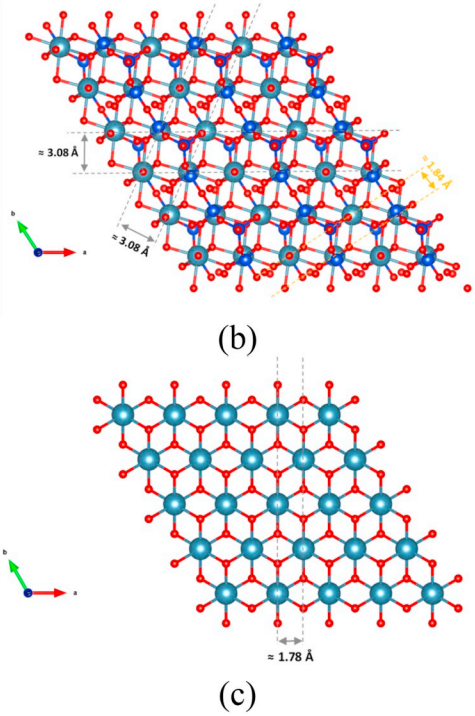

Fig. 3. Global X-ray diffraction spectra of organosilane-modified gels and TEOS C-S-H (a). Atomic structure of 11 Å tobermorite, monoclinic polytype, after Merlino et al. [44] (b), and structure of portlandite (c). Structural models generated in VESTA®.

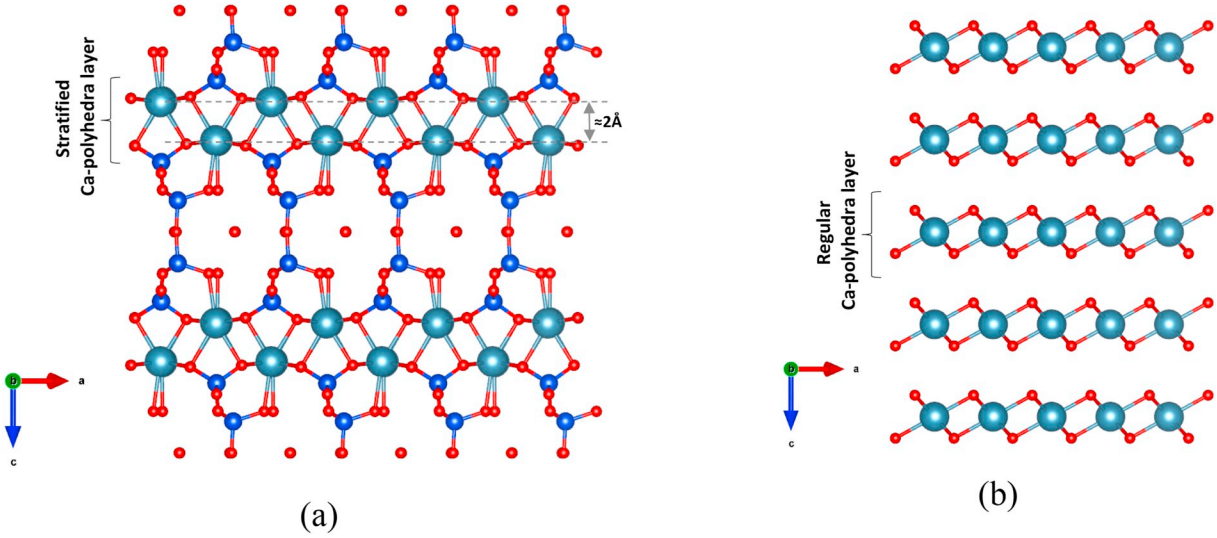

Fig. 4. Projections of the atomic structure on the surface normal to **b** unit cell vector: (a) 11 Å tobermorite (monoclinic type, Merlino et al. [44]) comprising a stratified layer of Ca polyhedra along **c**, (b) portlandite with uniform Ca polyhedral layer. Structural models generated in VESTA®.

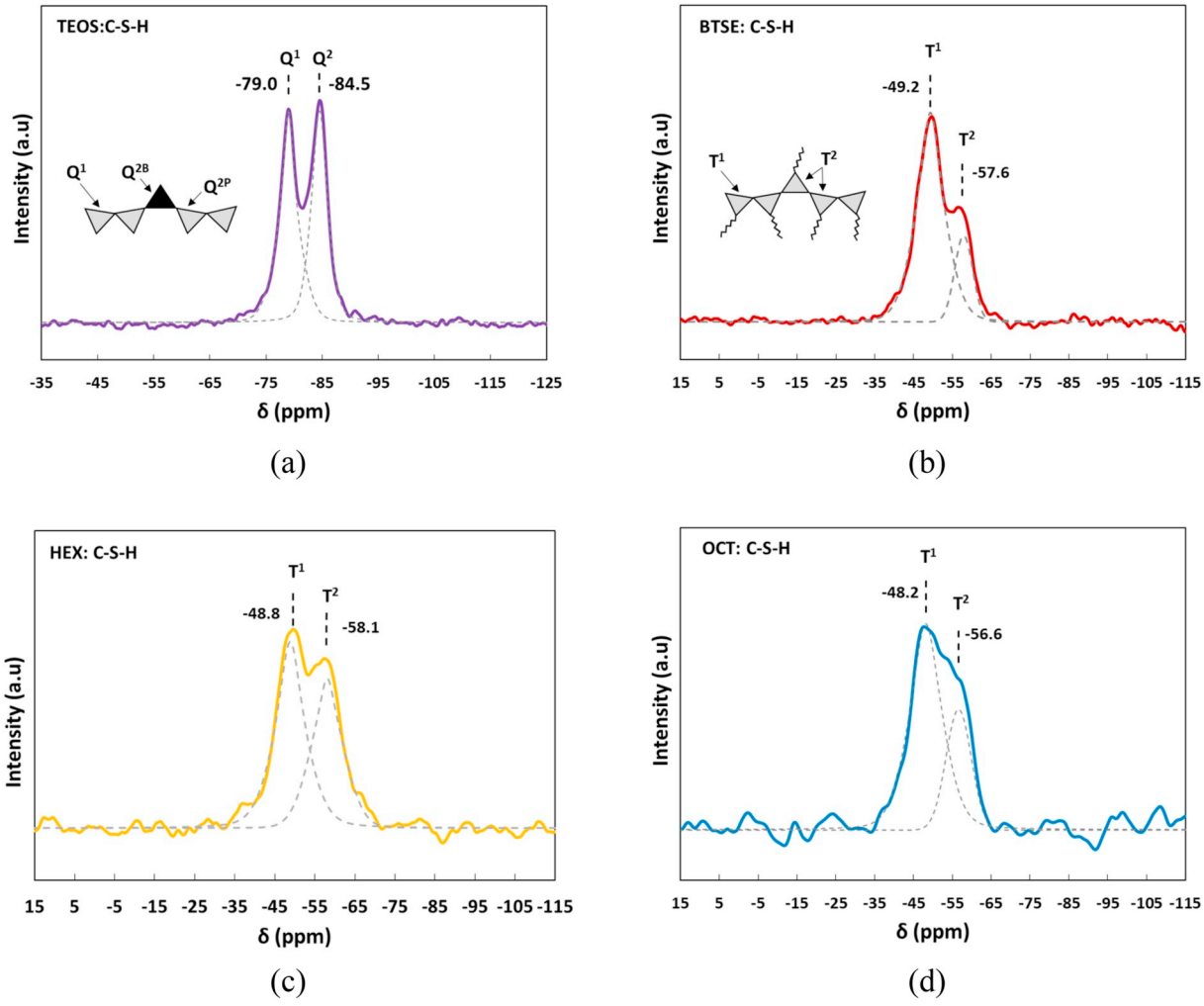

Fig. 5. ^{29}Si MAS NMR spectra obtained on: (a) TEOS: C-S-H, (b) BTSE: C-S-H, (c) HEX: C-S-H and (d) OCT: C-S-H hybrids. Results presented for spectra decomposition into two dominant species T^1 and T^2.

modifications, is provided by ^{29}Si NMR spectroscopy. The commonly used Q^n and T^n nomenclature is adopted. In this notation, Q represents the silicon atom bonded to four oxygen atoms forming tetrahedron while T represents the silicon atom bonded to three oxygen atoms and one organic group, R. The superscript *n* indicates the number of other Q, or T units attached to the tetrahedron under study [51,52].

Table 3
Estimates of ^{29} Si NMR relative intensities (%) of the investigated gel samples.

Gel type	Si – species (%)					
	Q^1	Q^2	T^0	T^1	T^2	T^3
TEOS:C-S-H	52.0	48.0	–	–	–	–
BTSE:C-S-H	–	–	(3.7)[a]	79.8 (72.0)	20.2 (23.4)	(0.9)
HEX:C-S-H	–	–	(5.6)[b]	57.0 (47.9)	43.0 (39.6)	(5.1)[b]
OCT:C-S-H	–	–	(4)	70.6 (56)	29.4 (40)	–

[a] () – values in the parenthesis represent estimates from NMR data decomposition including T^0 and/or T^3 peak.
[b] Estimate of significantly reduced certainty due to low signal-to-noise (S/N) ratio and high fluctuations on the background.

The reference C-S-H obtained from the synthesis with TEOS displays NMR spectrum (Fig. 5a), which has two maxima with chemical shifts, δ, centered around −79 ppm and − 85 ppm. The first peak is characteristic of the terminal silicate groups, Q^1, and the second corresponds to Q^2 sites both of which are present in the *dreierketten* chains running along **b** axis on the layers of calcium polyhedra [5,41,42,52–55]. The degree of silicate chain polymerization expressed as the mean chain length $2(1 + Q^2/Q^1)$ assuming Q^3 sites absent [39,42,43] is equal to 3.85. Consequently, the $Q^1/\Sigma Q^i$ ratio ($i = 1,2$) reflecting the contribution of Q^1 terminal sites approaches 52% (Table 3), and the fraction of tetrahedral sites that are vacant is ≈ 21%. Given this amount of vacant sites in the reference C-S-H gel the calculated Ca/Si ratio (following approach derived by Richardson [43]) is 1.10. This value compares well with the Ca/Si ratio of 1.03 measured in the elemental analysis by ICP-OES (Table 2). Such agreement additionally confirms the appropriateness of the selected sol-gel synthesis conditions, e.g. hydrolysis time and pH, as the target value of Ca/Si ratio of the C-S-H precipitate has been achieved (see Table 1).

The ^{29}Si NMR spectra of organic-inorganic calcium-silicate-hydrate gels are presented in Fig. 5b–d. Naturally, the domain of chemical shift changes: T0 – T3 sites have resonances in the approximate range {−40;-70} ppm referenced w.r.t liquid TMS (tetramethylsilane) [36,37,52,56]. In all three types of synthesized hybrid gels two dominant resonances are revealed, which correspond to T^1 (≈ − 49 ppm) and T^2 (≈ − 58 ppm) sites, respectively. This means the dominant T species in the organo-silicon network of hybrid gels are the ones characteristic of simple dimer structures or linear segments, e.g. trimer [51] (Table 3). However, as can be inferred from Fig. 5b, BTSE: C-S-H spectrum also displays a subtle shoulder located between −35 to −45 [ppm]. Given the approximate shift difference -10 ppm for every new tetrahedral attached [51] this range is typical for T^0 monomers [57–59]. If such shoulder is considered in the ^{29}Si NMR spectra decomposition, the estimated relative abundance of T^0 species in BTSE is 4% (Table 3). This estimate becomes significantly less reliable in the case of HEX:C-S-H and OCT:C-S-H gels. In both cases, the signal-to-noise ratio is drastically reduced and the variations on the background are of comparable magnitude to the intensity of the visible shoulders at

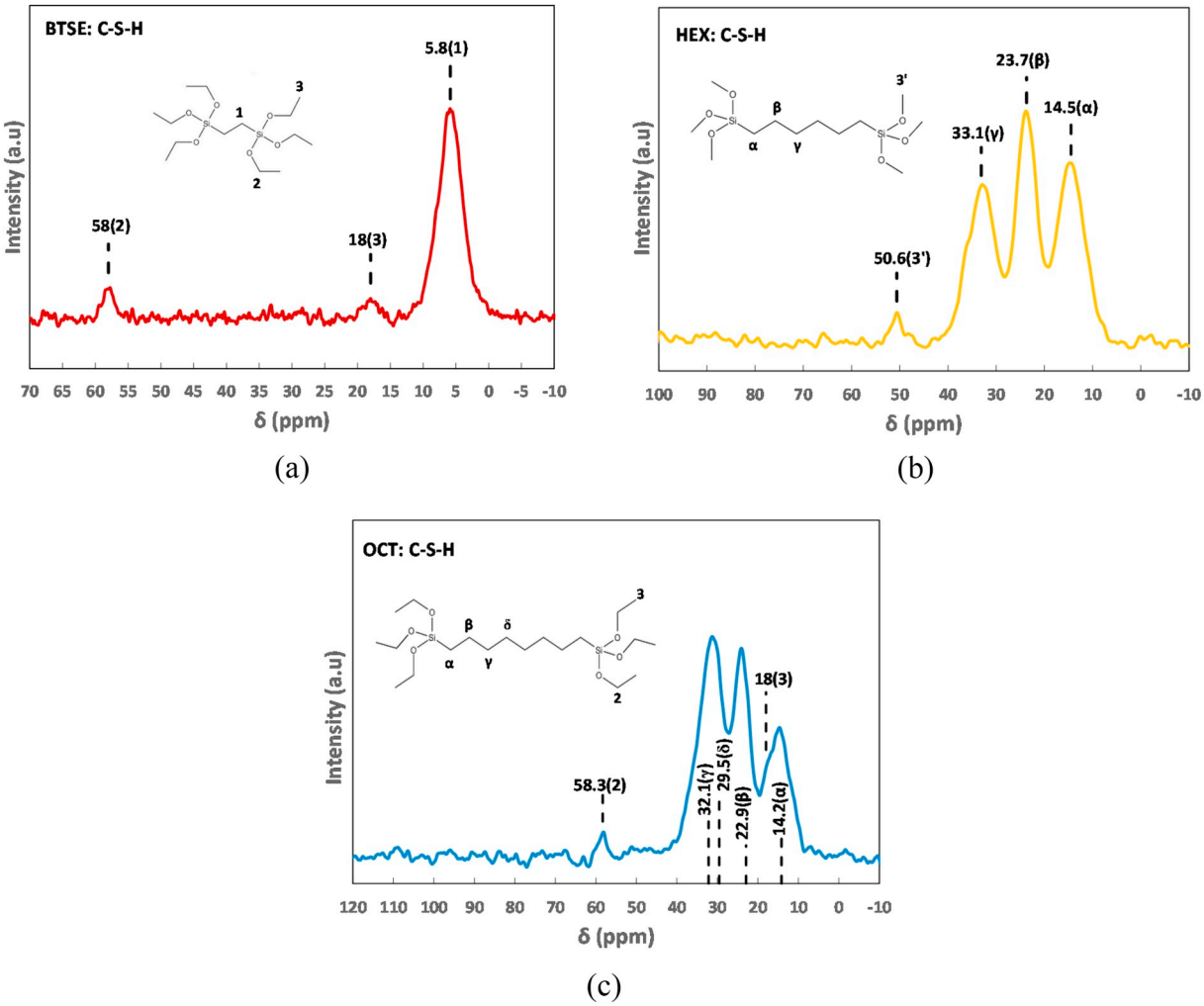

Fig. 6. ^{13}C CP-MAS NMR spectra obtained on: (a) BTSE: C-S-H, (b) HEX: C-S-H and (c) OCT: C-S-H hybrids. Reference lines in (c) mark resonances in octane (C_8H_{18}) in $CDCl_3$ solvent [63].

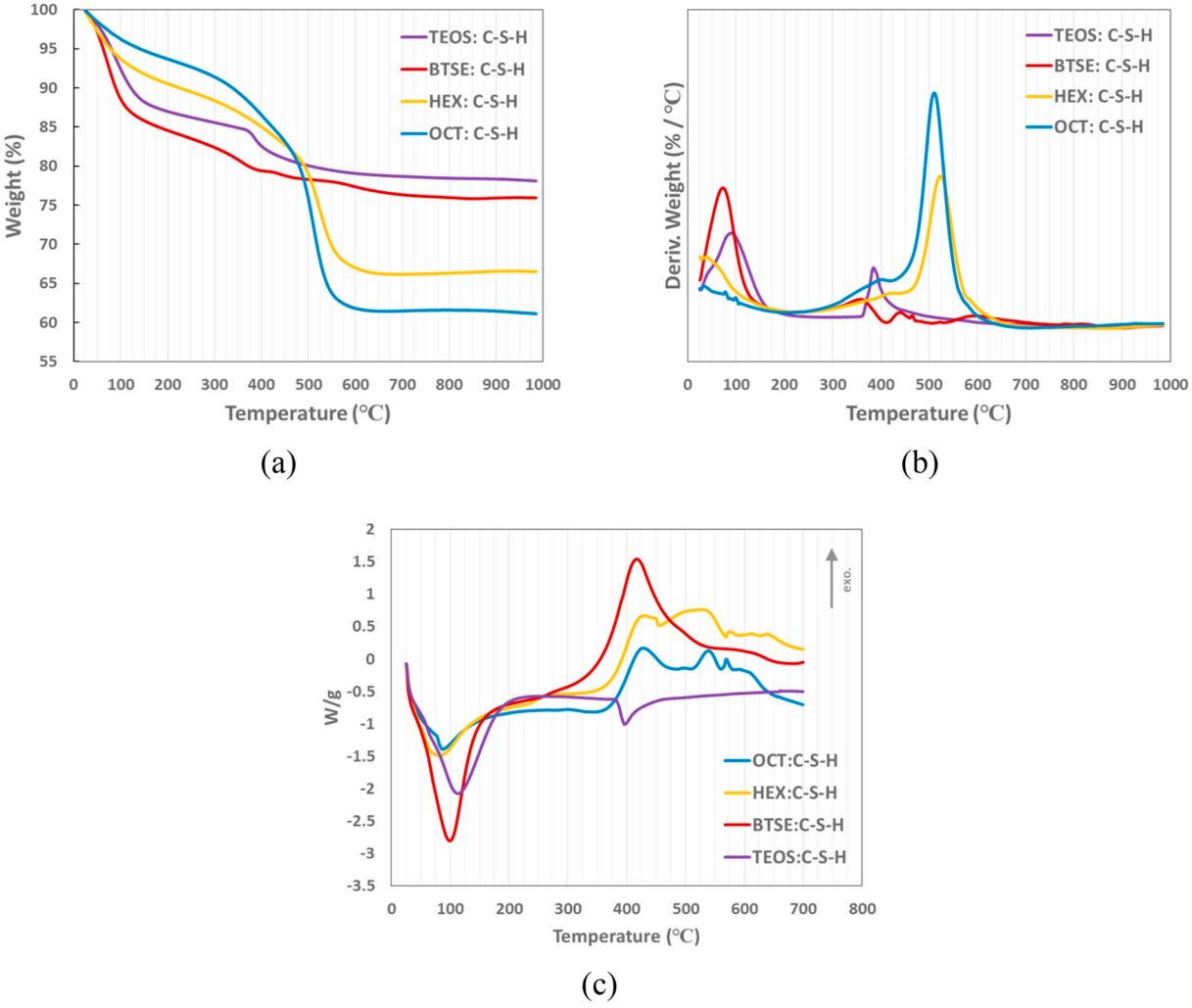

Fig. 7. TGA (a), DTG (b) and DSC (c) curves for inorganic and hybrid C-S-H gels. Curves recorded at a heating rate of °C/min in flowing N_2 atmosphere. Curves represent the average trends inferred from three tests.

Table 4
TGA weight loss (%) measured for inorganic and hybrid C-S-H gels.

Gel type	Temperature range (°C)		
	< 200	200–600	> 600
TEOS:C-S-H	13.0 ± 0.4	7.9 ± 0.2 (10.2 ± 0.3)	1.0 ± 0.1 (1.2 ± 0.1)
BTSE:C-S-H	15.4 ± 0.2	7.2 ± 0.1 (9.5 ± 0.1)	1.4 ± 0.1 (1.9 ± 0.1)
HEX:C-S-H[a]	9.5 ± 0.2	23.6 ± 0.5 (35.0 ± 1.0)	0.5 ± 0.1 (0.7 ± 0.2)
OCT:C-S-H	6.0 ± 2.0	31.8 ± 0.3 (52.0 ± 2.0)	0.7 ± 0.1 (1.1 ± 0.2)

[a] Values in the parenthesis reported relative to the ignited weight.

T^0 and/or T^3 resonances (see Fig. 5c). Therefore, these results must be interpreted with caution.

The ^{13}C CP-MAS NMR spectra of organic-inorganic calcium silicate hydrate gels, which are presented in Fig. 6, indicate the undisturbed structure of alkyl chain and chemical stability of Si—C bond. Accordingly, BTSE hybrid gel shows three resonance bands centered at 5.8 ppm, 18 ppm and 58 ppm. The first resonance is attributed to ethane carbon atoms in the organic chain framework [60]. Remaining peaks relate to the C atoms in the residual functional ethoxy groups (CH_3CH_2O–) which did not hydrolyze [51,61]. A resonance triplet {14.5; 23.7; 33.1} ppm of C atoms is observed in HEX: C-S-H gel (see Fig. 6b). Such triplet is a common feature of carbon atoms incorporated in the 1,6-bis(trimethoxysilyl) hexane internal chain (labeled as α, β and γ) [62]. Similarly, a small resonance is recorded at 50.6 ppm and it originates from the unhydrolyzed methoxy (CH_3O–) groups [62]. Finally, spectra observed in OCT: C-S-H gel displays three main maxima which are the convolution of resonances of C atoms in alkyl chain [63,64] and in residual ethoxy groups.

3.4. TGA/DTG and DSC analysis

Thermal behavior of all synthesized gels was examined in the thermogravimetric analysis. Moreover, to gain insight into the energetic character of the observed changes, e.g. endothermic vs. exothermic process, DSC calorimetry was applied.

For all gels, a steep weight loss is observed from the initial temperature to approximately 200 °C (see Fig. 7). In this temperature interval, the weight loss is primarily driven by the removal of free water present in the capillary and gel pores, as well as the volatilization of water weakly bound to the surface [1,42,43,46,65]. Moreover, in the case of inorganic C-S-H, e.g. 14 Å tobermorite, jennite, drying at temperatures above ≈70 °C tends to also remove the interlayer water molecules [45,66]. In all cases, the weight loss in the low temperature range is an endothermic process as confirmed by DSC measurements (Fig. 7c).

The second prominent changes recorded with TGA take place in the approximate temperature range 200 °C to 600 °C. However, in this particular case, the nature of the process leading to the weight decline

is quite different for inorganic and hybrid gels. Accordingly, TEOS: C-S-H displays an abrupt decline which peaks at 390 °C (see Fig. 7b) and the peak intensity is steadily decaying to 600 °C. The DSC signal indicates the endothermic nature of this process (Fig. 7c), which suggests dehydroxylation. It must be mentioned, the DTG peak location quite closely corresponds to the dehydration temperature of portlandite, $Ca(OH)_2$. Depending on its particle size, the degree of crystallinity, as well as the heating rate the peak temperature of portlandite decomposition varies from 400 °C to 460 °C [67,68]. However, the X-ray diffraction measurements performed in this study (Fig. 3a) showed no trace of C-S-H contamination with portlandite phase. A similar observation was reported by Kunther [69] and Marty [70] who attributed this phenomenon to microcrystalline portlandite in the C-S-H (Ca/Si = 1), which is intimately mixed with C-S-H. Such intermixing of the nano-sized CH, in the form of lamellae type microcrystals ~10 nm thick, was directly observed with TEM microscopy in Portland cement pastes of low water/cement ratio [71]. Finally, the $Ca(OH)_2$ contamination of synthetic C-S-H gels is frequently reported for solids with Ca/Si ratio approaching 1.5, corresponding to the solubility limit of CH [39,69,72,73]. Although not tested here, another plausible explanation for this observed weight loss is the dehydroxylation of the C-S-H gel itself. Such hypothesis was postulated by Beaudoin [25], and draws its analogy from the intermediate-temperature reaction of clay minerals. Interestingly, jennite phase which is considered as one of two model compounds of C-S-H displays a broad endotherm and weight loss in the range from 360 °C to 460 °C which corresponds to its transformation to disordered phase [45].

The weight loss observed in the hybrid organic-inorganic C-S-H gels between 200 °C and 600 °C (Fig. 7a-b) is characteristic of decomposition of organic $[CH_2]_n$ chains [56,61,74–77]. At this temperature, the organic framework decomposes in the process of pyrolysis. As indicated by DSC signal, this process is exothermic (Fig. 7c). Additionally, the DTG curves display more than one maxima in all gels and the peak intensity increases with the increasing molecular weight (or equivalently alkyl chain length) of the organosilane used in the synthesis. Consequently, the same trend is observed in the weight loss curve (Fig. 7a, Table 4).

3.5. TEM and particle morphology

The bright-field TEM electron micrographs of the organic-inorganic solid with the longest alkyl chain, OCT:C-S-H, are presented in Fig. 8. As previously suggested by the results of X-ray powder diffraction (Fig. 3), the nano-sized particles show plate-like morphology at the smallest

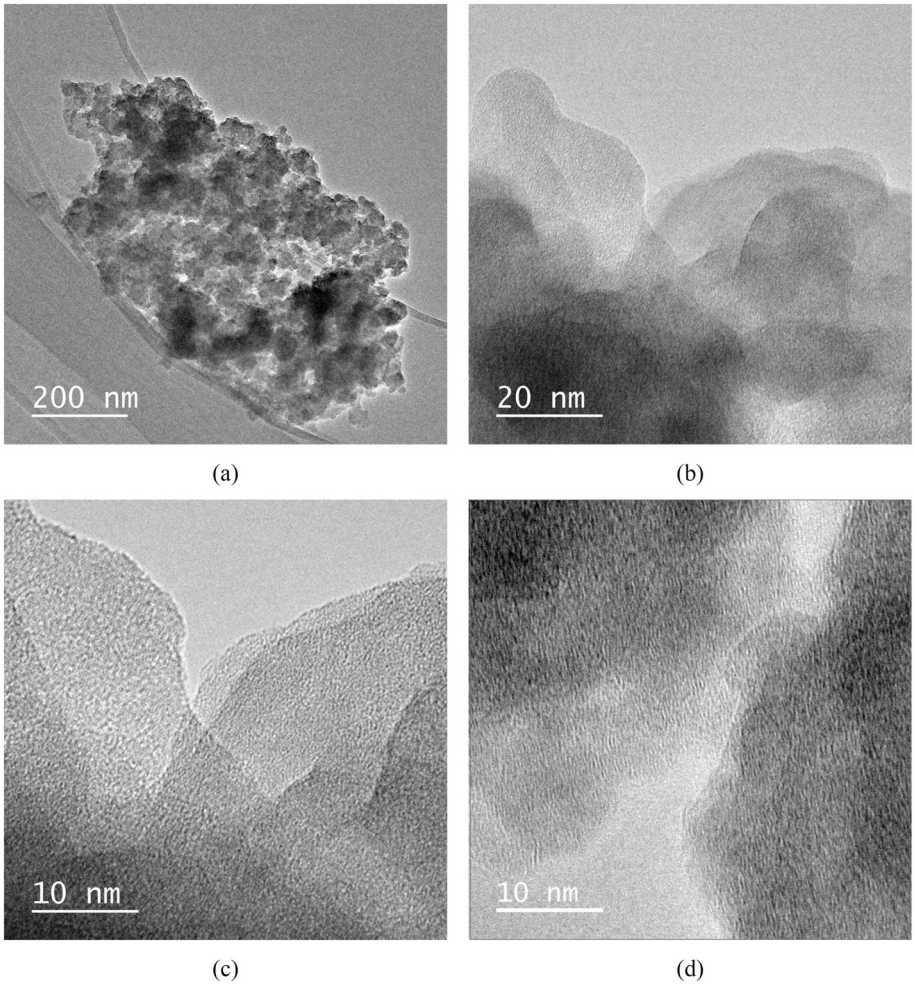

Fig. 8. TEM micrographs of the OCT: C-S-H hybrid calcium silicate gel: a) large cluster of numerous aggregates composed of multiple stacked 2D sheets (b-e).

scale (Fig. 8b-c). From this perspective, its particle morphology is quite similar to the morphology of low-lime C-S-H, e.g. tobermorite, which is known to be crystallized in the form of thin plates or laths. The selected area diffraction examination run on multiple particles showed broad halo characteristic of amorphous materials, however, on several occasions, a subtle intensity hunch in the approximate range 2.5 Å – 3.6 Å could be inferred. Plate-like particles show a clear tendency toward stacking and forming larger size agglomerates with periodicity in the normal direction to the image plane, **c**-direction, (Fig. 8a and c).

4. Summary and conclusions

This work investigated the novel approach to nano-scale cross-linking of C-S-H, the primary binder of concrete, through hydrolysis and condensation of functionalized bis-alkoxysilanes. For this purpose, organic-inorganic C-S-H gels were synthesized via sol-gel processing with organosilanes of alkyl [CH_2]-n chain size ranging from 2 to 8. All gels were subject to scrutinized multi-technique characterization, which included mass spectrometry, X-ray diffraction, solid state ^{29}Si and ^{13}C NMR, thermogravimetry and electron microscopy. Additionally, a reference inorganic C-S-H gel, with Ca/Si = 1, was synthesized.

The successful incorporation of organometallic molecules into the molecular structure of organic-inorganic calcium silicate hydrate gels has been confirmed with X-ray powder diffraction results, which showed a systematic shift in the d_{002} basal reflection toward smaller diffraction angle for longer alkyl [CH_2]-n chain organosilanes. Such shift reflects the increasing interlayer spacing, in the molecular framework of hybrid C-S-H gels, which must be realized in order to accommodate longer chain molecules with silanol bonds condensing on the opposite Ca-galleries. However, it was also revealed that the incorporation of bis-organosilanes significantly affects the long range structural order in the **a-b** plane. The observed differences between reference and hybrid C-S-H gels point toward the layered hexagonal Ca-polyhedra arrangement in hybrid gels and nanocrystalline turbostratic structure. The layered nature of hybrid gels was additionally supported by electron micrographs revealing the stacks of nano-scale plate-like precipitate. Moreover, interlayer spacing in hybrid gels does not contract upon dehydration from 50 °C up to 105 °C, indicating no shrinkage along **c**-direction.

The condensation of silanol bonds of organosilanes results in the two dominant resonances (T^1 and T^2) observed in ^{29}Si MAS NMR spectra, regardless of the size of alkyl [CH_2]-n chain. Therefore, the silanol bonds condensing on the Ca-polyhedra layer tend to establish simple dimer, or trimer, segments. The ^{13}C CP-MAS NMR confirmed the presence of resonances characteristic of carbon atoms in the organic chain framework. The presence of the organic framework was confirmed in the thermal analysis which showed pyrolysis of alkyl chains in the approximate range 200 °C to 600 °C.

CRediT authorship contribution statement

Amir Moshiri:Investigation, Formal analysis, Validation, Methodology, Writing - review & editing.**Damian Stefaniuk**:Methodology, Software, Formal analysis.**Scott K. Smith**:Methodology, Formal analysis, Investigation, Writing - review & editing.**Ali Morshedifard**:Formal analysis, Writing - review & editing.**Debora Frigi Rodrigues**:Funding acquisition, Resources, Writing - review & editing.**Mohammad Javad Abdolhosseini Qomi**:Conceptualization, Writing - original draft, Funding acquisition, Formal analysis, Methodology.**Konrad J. Krakowiak**:Conceptualization, Writing - original draft, Funding acquisition, Formal analysis, Methodology, Project administration, Resources, Supervision.

Acknowledgment

This work was supported by the National Science Foundation under Grants No. 1825921, 1826122, The Welch Foundation award No.E-2011-20190330. The research team is grateful for valuable discussions with Dr. Sylvain Grangeon and Dr. Francis Claret, French Geological Survey (BRGM), as well as Dr. Charles Settens, Materials Research Laboratory, Massachusetts Institute of Technology.

References

[1] S. Mindess, J.F. Young, D. Darwin, Concrete, second ed., Prentice Hall, 2002.
[2] P.K. Mehta, P.J.M. Monteiro, Concrete: Microstructure, Properties, and Materials, third ed., McGraw-Hill, New York, 2006.
[3] M.J. Abdolhosseini Qomi, K.J. Krakowiak, M. Bauchy, K.L. Stewart, R. Shahsavari, D. Jagannathan, D.B. Brommer, A. Baronnet, M.J. Buehler, S. Yip, F.-J. Ulm, K.J. Van Vliet, R.J.-M. Pellenq, Combinatorial molecular optimization of cement hydrates, Nat. Commun. 5 (2014) 4960. https://doi.org/https://doi.org/10.1038/ncomms5960.
[4] M.J. Abdolhosseini Qomi, F.-J. Ulm, R.J.-M. Pellenq, Evidence on the dual nature of aluminum in the calcium-silicate-hydrates based on atomistic simulations, J. Am. Ceram. Soc. 95 (2012) 1128–1137 https://doi.org/10.1111/j.1551-2916.2011.05058.x.
[5] G. Geng, R.J. Myers, M.J. Abdolhosseini Qomi, P.J.M. Monteiro, Densification of the interlayer spacing governs the nanomechanical properties of calcium-silicate-hydrate, Sci. Rep. 7 (2017) 10986. https://doi.org/https://doi.org/10.1038/s41598-017-11146-8.
[6] C. Plassard, E. Lesniewska, I. Pochard, A. Nonat, Nanoscale experimental investigation of particle interactions at the origin of the cohesion of cement, Langmuir 21 (2005) 7263–7270 https://doi.org/10.1021/la050440+.
[7] M. Bauchy, B. Wang, M. Wang, Y. Yu, M.J. Abdolhosseini Qomi, M.M. Smedskjaer, Ch. Bichara, F.-J. Ulm, R.-J.M. Pellenq, Fracture toughness anomalies: viewpoint of topological constraint theory, Acta Mater. 121 (2016) 234–239 https://doi.org/10.1016/j.actamat.2016.09.004.
[8] F. Pelisser, P.J.P. Gleize, A. Mikowski, Effect of the Ca/Si molar ratio on the micro/nanomechanical properties of synthetic C-S-H measured by nanoindentation, J. Phys. Chem. C 116 (2012) 17219–17227 https://doi.org/10.1021/jp302240c.
[9] A. Morshedifard, S. Masoumi, M.J. Abdolhosseini Qomi, Nanoscale origins of creep in calcium silicate hydrates, Nat. Commun. 9 (2018), 1785, https://doi.org/https://doi.org/10.1038/s41467-018-04174-z.
[10] R.J.-M. Pellenq, N. Lequeux, H. van Damme, Engineering the bonding scheme in C-S-H: the iono-covalent framework, Cem. Concr. Res. 38(2) (2008) 159–174. https://doi.org/https://doi.org/10.1016/j.cemconres.2007.09.026.
[11] A. Gmira, J. Minet, A. Francischini, N. Lequeux, R.J.-.M. Pellenq, H. Van Damme, Molecular engineering of the cohesion in neat and hybrid cement hydrates, Proceedings of ACI Session on "Nanotechnology of Concrete: Recent Developments and Future Perspectives", Denver, 2006, pp. 29–40.
[12] M.J. Abdolhosseini Qomi, F.-J. Ulm, R.J.-.M. Pellenq, Physical origins of thermal properties of cement paste, Phys. Rev. Applied. 3 (2015) 064010, , https://doi.org/10.1103/PhysRevApplied.3.064010.
[13] Y. Zhou, A. Morshedifard, J. Lee, M.J. Abdolhosseini Qomi, The contribution of propagons and diffusons in heat transport through calcium-silicate-hydrates, Appl. Phys. Lett. 110 (2017) 043104, , https://doi.org/10.1063/1.4975159.
[14] M.D. Losego, I.P. Blitz, R.A. Vaia, D.G. Cahill, P.V. Braun, Ultralow thermal conductivity in organoclay nanolaminates synthesized via simple self-assembly, Nano Lett. 13 (2013) 2215–2219, https://doi.org/10.1021/nl4007326.
[15] J.P. Randall, M.A.B. Meador, S.C. Jana, Tailoring mechanical properties of aerogels for aerospace applications, ACS Appl. Mater. Interfaces 3 (2011) 613–626, https://doi.org/10.1021/am200007n.
[16] H. Matsuyama, J.F. Young, Intercalation of polymers in calcium silicate hydrate: a new synthetic approach to biocomposites? Chem. Mater. 11 (1999) 16–19, https://doi.org/10.1021/cm980549l.
[17] H. Matsuyama, J.F. Young, Synthesis of calcium silicate hydrate/polymer complexes: part I. anionic and nonionic polymers, J. Mater. Res. 14 (1999) 3379–3388, https://doi.org/10.1557/JMR.1999.0458.
[18] H. Matsuyama, J.F. Young, Synthesis of calcium silicate hydrate/polymer complexes: part II. Cationic polymers and complex formation with different polymers, J. Mater. Res. 14 (1999) 3389–3396, https://doi.org/10.1557/JMR.1999.0459.
[19] S.C. Mojumdar, L. Raki, Preparation and properties of calcium silicate hydrate-poly (vinyl alcohol) nanocomposite materials, J. Therm. Anal. Calorim. 82 (2005) 89–95, https://doi.org/10.1007/s10973-005-0846-8.
[20] F. Merlin, H. Lombois, S. Joly, N. Lequeux, J.-L. Halary, H. Van Damme, Cement-polymer and clay-polymer nano- and meso-composites: spotting the difference, J. Mater. Chem. 12 (2002) 3308–3315, https://doi.org/10.1039/B205279M.
[21] F. Pelisser, P.J.P. Gleize, A. Mikowski, Structure and micro-nanomechanical characterization of synthetic calcium-silicate-hydrate with poly(vinyl)alcohol, Cem. Concr. Comp. 48 (2014) 1–8. https://doi.org/https://doi.org/10.1016/j.cemconcomp.2014.01.004.
[22] Y. Zhou, L. Tang, J. Liu, Ch. Miao, Interaction mechanisms between organic and inorganic phases in calcium silicate hydrates / poly(vinyl alcohol) composites, Cem. Conr. Res. 125 (2019) 105891, , https://doi.org/10.1016/j.cemconres.2019.105891.

[23] J.J. Beaudoin, L. Raki, R. Alizadeh, A ^{29}Si MAS NMR study of modified C-S-H nanostructures, Cem. Con. Comp. 31 (2009) 585–590, https://doi.org/10.1016/j.cemconcomp.2008.11.004.

[24] J.J. Beaudoin, H. Dramé, L. Raki, R. Alizadeh, Formation and properties of C-S-H–PEG nano-structures, Mater. Struct. 42 (2009) 1003–1014, https://doi.org/10.1617/s11527-008-9439-x.

[25] J.J. Beaudoin, H. Dramé, L. Raki, R. Alizadeh, Formation and characterization of calcium silicate hydrate–hexadecyltrimethylammonium nanostructure, J. Mater. Res. 23 (2008) 2804–2815, https://doi.org/10.1557/JMR.2008.0342.

[26] V. Kanchanason, J. Plank, Role of pH on the structure, composition and morphology of CSH–PCE nanocomposites and their effect on early strength development of Portland cement, Cem. Concr. Res. 102 (2017) 90–98, https://doi.org/10.1016/j.cemconres.2017.09.002.

[27] R. Alizadeh, J.J. Beaudoin, L. Raki, V. Terskikh, C-S-H/polyaniline nanocomposites prepared by in-situ polymerization, J. Mater. Sci. 46 (2011) 460–467, https://doi.org/10.1007/s10853-010-4918-1.

[28] E.P. Giannelis, R. Krishnamoorti, E. Manias, Polymer-silicate nanocomposites: model systems for confined polymers and polymer brushes, Polymers in Confined Environments, Springer, Berlin, Heidelberg, 1999, pp. 107–147.

[29] A. Popova, G. Geoffroy, M.-F. Renou-Gonnord, P. Faucon, E. Gartner, Interactions between polymeric dispersants and calcium silicate hydrates, J. Am. Ceram. Soc. 83 (2000) 2556–2560, https://doi.org/10.1111/j.1151-2916.2000.tb01590.x.

[30] J. Ha, S. Chae, K.W. Chou, T. Tyliszczak, P.J.M. Monteiro, Effect of polymers on the nanostructure and on the carbonation of calcium silicate hydrates: a scanning transmission X-ray microscopy study, J. Mater. Sci. 47 (2012) 976–989, https://doi.org/10.1007/s10853-011-5877-x.

[31] R. Khoshnazar, J.J. Beaudoin, L. Raki, A. Alizadeh, Characteristics and engineering performance of C-S-H/Aminobenzoic acid composite systems, J. Adv. Concr. Technol. 13 (2015) 415–420, https://doi.org/10.3151/jact.13.415.

[32] S.C. Mojumdar, L. Raki, Preparation, thermal, spectral and microscopic studies of calcium silicate hydrate poly(acrylic acid) nanocomposite materials, J. Therm. Anal. Calorim. 85 (2006) 99–105, https://doi.org/10.1007/s10973-005-7353-9.

[33] F. Pelisser, P.J.P. Gleize, A. Mikowski, Effect of poly(diallyldimethylammonium chloride) on nanostructure and mechanical properties of calcium silicate hydrate, Mater. Sci. Eng. A 527 (2010) 7045–7049, https://doi.org/10.1016/j.msea.2010.07.057.

[34] P.G. Pape, Adhesion promoters: Silane coupling agents, in: M. Kutz (Ed.), Applied Plastics Engineering Handbook, Elsevier, 2017, pp. 555–572, , https://doi.org/10.1016/B978-0-323-39040-8.00026-2.

[35] L. Ukrainczyk, R.A. Bellman, A.B. Anderson, Template synthesis and characterization of layered Al- and Mg-silsesquioxanes, J. Phys. Chem. B 101 (1997) 531–539, https://doi.org/10.1021/jp962937l.

[36] J. Minet, S. Abramson, B. Bresson, C. Sanchez, V. Montouillot, N. Lequeux, New layered calcium organosilicate hybrids with covalently linked organic functionalities, Chem. Mater. 16 (2004) 3955–3962, https://doi.org/10.1021/cm034967o.

[37] J. Minet, S. Abramson, B. Bresson, A. Franceschini, H. Van Damme, N. Lequeux, Organic calcium silicate hydrate hybrids: a new approach to cement based nanocomposites, J. Mater. Chem. 16 (2006) 1379–1383, https://doi.org/10.1039/B515947D.

[38] A. Franceschini, S. Abramson, V. Mancini, B. Bresson, Ch. Chassenieux, N. Lequeux, New covalent bonded polymer–calcium silicate hydrate composites, J. Mater. Chem. 17 (2007) 913–922, https://doi.org/10.1039/B613077A.

[39] J.J. Chen, J.J. Thomas, H.F.W. Taylor, H.M. Jennings, Solubility and structure of calcium silicate hydrate, Cem. Concr. Res. 34 (9) (2004) 1499–1519, https://doi.org/10.1016/j.cemconres.2004.04.034.

[40] R.W. Murray, D.J. Miller, K.A. Kryc, Analysis of major and trace elements in rocks, sediments, and interstitial waters by inductively coupled plasma-atomic emission spectrometry (ICP-AES), ODP Tech. Note. 29 (2000) 1–27, https://doi.org/10.2973/odp.tn.29.2000.

[41] I.G. Richardson, The calcium silicate hydrates, Cem. Concr. Res. 38 (2) (2008) 137–158, https://doi.org/10.1016/j.cemconres.2007.11.005.

[42] H.F.W. Taylor, Cement Chemistry, second ed., Thomas Telford, London, 1997.

[43] I.G. Richardson, Model structures for C-(A)-S-H(I), Acta Cryst 70 (2014) 903–923, https://doi.org/10.1107/S2052520614021982.

[44] S. Merlino, E. Bonaccorsi, T. Armbruster, Tobermorites: their real structure and order-disorder (OD) character, Am. Mineral. 84 (10) (1999) 1613–1621, https://doi.org/10.2138/am-1999-1015.

[45] P. Yu, R.J. Kirkpatrick, Thermal dehydration of tobermorite and jennite, Concr. Sci. Eng. 1 (1999) 185–191.

[46] H.F.W. Taylor, Bound water in cement pastes and its significance for pore solution compositions, MRS Proc. 85 (1986) 47–54, https://doi.org/10.1557/PROC-85-47.

[47] H. Matsuyama, J.F. Young, Effects of pH on precipitation of quasi-crystalline calcium silicate hydrate in aqueous solution, Adv. Cem. Res. 12 (2000) 29–33, https://doi.org/10.1680/adcr.2000.12.1.29.

[48] S. Grangeon, F. Claret, Y. Linard, C. Chiaberge, X-ray diffraction: a powerful tool to probe and understand the structure of nanocrystalline calcium silicate hydrates, Acta Cryst 69 (2013) 465–473, https://doi.org/10.1107/S2052519213021155.

[49] S. Grangeon, F. Claret, C. Roosz, T. Sato, S. Gaboreau, Y. Linard, Structure of nanocrystalline calcium silicate hydrates: insights from X-ray diffraction, synchrotron X-ray absorption and nuclear magnetic resonance, J. Appl. Crystallogr. 49 (2016) 771–783, https://doi.org/10.1107/S1600576716003885.

[50] S. Grangeon, B. Lanson, M. Lanson, A. Manceau, Crystal structure of Ni-sorbed synthetic vernadite: a powder X-ray diffraction study, Mineral. Mag. 72 (6) (2008) 1279–1291, https://doi.org/10.1180/minmag.2008.072.6.1279.

[51] G. Engelhardt, D. Michel, High-Resolution Solid-State NMR of Silicates and Zeolites, John Wiley & Sons, 1987.

[52] R.H. Glaser, G.L. Wilkes, Ch.E. Bronnimann, Solid-state ^{29}Si NMR of TEOS-based multifunctional sol-gel materials, J. Non-Cryst. Solids 113 (1989) 73–87, https://doi.org/10.1016/0022-3093(89)90320-7.

[53] X. Cong, R.J. Kirkpatrick, ^{29}Si MAS NMR study of the structure of calcium silicate hydrate, Adv. Cem. Based Mater. 3 (1996) 144–156, https://doi.org/10.1016/S1065-7355(96)90046-2.

[54] I.G. Richardson, Tobermorite/jennite- and tobermorite/calcium hydroxide-based models for the structure of C-S-H: applicability to hardened pastes of tricalcium silicate, β-dicalcium silicate, Portland cement, and blends of Portland cement with blast-furnace slag, metakaolin, or silica fume, Cem. Con. Res. 34 (2004) 1733–1777, https://doi.org/10.1016/j.cemconres.2004.05.034.

[55] E. Pustovgar, R.P. Sangodkar, A.S. Andreev, M. Palacios, B.F. Chmelka, R.J. Flatt, J.-B. d'Espinose de Lacaillerie, Understanding silicate hydration from quantitative analyses of hydrating tricalcium silicates, Nat. Com. 7 (2016) 10952, , https://doi.org/10.1038/ncomms10952.

[56] Y.-H. Han, A. Taylor, M.D. Mantle, K.M. Knowles, Sol-gel-derived organic-inorganic hybrid materials, J. Non-Cryst. Solids 353 (2007) 313–320, https://doi.org/10.1016/j.jnoncrysol.2006.05.042.

[57] Y. Sugahara, S. Okada, S. Sato, K. Kuroda, C. Kato, ^{29}Si-NMR study of hydrolysis and initial polycondensation processes of organoalkoxysilanes. II. Methyltriethoxysilane, J. Non-Cryst. Solids 167 (1994) 21–28, https://doi.org/10.1016/0022-3093(94)90362-X.

[58] J. Sanchez, S.E. Rankin, A.V. McCormick, ^{29}Si NMR kinetic study of tetraethoxysilane and ethyl-substituted ethoxysilane polymerization in acidic conditions, Ind. Eng. Chem. Res. 35 (1996) 117–129, https://doi.org/10.1021/ie950246q.

[59] S.K. Young, W.L. Jarrett, K.A. Mauritz, Nafion®/ORMOSIL nanocomposites via polymer-in situ sol–gel reactions. 1. Probe of ORMOSIL phase nanostructures by ^{29}Si solid-state NMR spectroscopy, Polymer 43 (2002) 2311–2320, https://doi.org/10.1016/S0032-3861(02)00027-7.

[60] B.J. Melde, B.T. Holland, Ch.F. Blanford, A. Stein, Mesoporous sieves with unified hybrid inorganic/organic frameworks, Chem. Mater. 11 (1999) 3302–3308, https://doi.org/10.1021/cm9903935.

[61] K. Karadag, I. Yati, H.B. Sonmez, Effective clean-up of organic liquid contaminants including BTEX, fuels, and organic solvents from the environment by poly(alkoxysilane) sorbents, J. Env. Man. 174 (2016) 45–54, https://doi.org/10.1016/j.jenvman.2016.01.043.

[62] D.A. Loy, K.A. Obrey-DeFriend, K.V. Wilson Jr., M. Minke, B.M. Baugher, C.R. Baugher, D.A. Schneider, G.M. Jamison, K.J. Shea, Influence of the alkoxide group, solvent, catalyst, and concentration on the gelation and porosity of hexylene-bridged polysilsesquioxanes, J. Non-Cryst. Solids 362 (2013) 82–94, https://doi.org/10.1016/j.jnoncrysol.2012.11.021.

[63] Spectral Database for Organic Compounds SDBS, National Institute of Advanced Industrial Science and Technology, https://sdbs.db.aist.go.jp/sdbs/cgi-bin/direct_frame_top.cgi.

[64] M. Khiterer, D.A. Loy, Ch.J. Cornelius, C.H. Fujimoto, J.H. Small, T.M. McIntire, K.J. Shea, Hybrid polyelectrolyte materials for fuel cell applications: design, synthesis, and evaluation of proton-conducting bridged polysilsesquioxanes, Chem. Mater. 18 (2006) 3665–3673, https://doi.org/10.1021/cm060440a.

[65] C. Roosz, S. Gaboreau, S. Grangeon, D. Prêt, V. Montouillout, N. Maubec, S. Ory, P. Blanc, P. Vieillard, P. Henocq, Distribution of water in synthetic calcium silicate hydrates, Langmuir 32 (2016) 6794–6805, https://doi.org/10.1021/acs.langmuir.6b00878.

[66] C. Biagioni, E. Bonaccorsi, M. Lezzerini, M. Merlini, S. Merlino, Thermal behaviour of tobermorite from N'Chwaning II mine (Kalahari Manganese Field, Republic of South Africa). I. Thermo-gravimetric and X-ray diffraction studies, Eur. J. Mineral. 24 (6) (2012) 981–989, https://doi.org/10.1127/0935-1221/2012/0024-2238.

[67] J.J. Beaudoin, T. Sato, P.J. Tumidajski, The thermal decomposition of $Ca(OH)_2$ polymorphs, in: J. Marchand, B. Bissonnette, R. Gagné, M. Jolin, F. Paradis (Eds.), 2nd International RILEM Symposium on Advances in Concrete Through Science and Engineering, Québec City, Canada, 2006, pp. 3–13.

[68] M. Khachani, A. El Hamidi, M. Halim, S. Arsalane, Non-isothermal kinetic and thermodynamic studies of the dehydroxylation process of synthetic calcium hydroxide $Ca(OH)_2$, J. Mater. Environ. Sci. 5 (2) (2014) 615–624.

[69] W. Kunther, S. Ferreiro, J. Skibsted, Influence of the Ca/Si ratio on the compressive strength of cementitious calcium-silicate-hydrate binders, J. Mater. Chem. A 5 (2017) 17401–17412, https://doi.org/10.1039/C7TA06104H.

[70] N.C.M. Marty, S. Grangeon, F. Warmont, C. Lerouge, Alteration of nanocrystalline calcium silicate hydrate (C-S-H) at pH 9.2 and room temperature: a combined mineralogical and chemical study, Mineral. Mag. 79 (2015) 437–458, https://doi.org/10.1180/minmag.2015.079.2.20.

[71] G.W. Groves, Microcrystalline calcium hydroxide in Portland cement pastes of low water/cement ratio, Cem. Concr. Res. 11 (1981) 713–718, https://doi.org/10.1016/0008-8846(81)90029-6.

[72] E.T. Rodriguez, K. Garbev, D. Merz, L. Black, I.G. Richardson, Thermal stability of C-S-H phases and applicability of Richardson and Groves' and Richardson C-(A)-S-H (I) models to synthetic C-S-H, Cem. Concr. Res. 93 (2017) 45–56, https://doi.org/10.1016/j.cemconres.2016.12.005.

[73] J.J. Kim, E.M. Foley, M.M. Reda Taha, Nano-mechanical characterization of synthetic calcium–silicate–hydrate (C–S–H) with varying CaO/SiO_2 mixture ratios,

Cem. Concr. Comp. 36 (2013) 65–70, https://doi.org/10.1016/j.cemconcomp.2012.10.001.
[74] M.C. Burleigh, M.A. Markowitz, M.S. Spector, B.P. Gaber, Direct synthesis of periodic mesoporous organosilicas: functional incorporation by co-condensation with organosilanes, J. Phys. Chem. B 105 (2001) 9935–9942, https://doi.org/10.1021/jp011814k.
[75] M.A. Wahab, W. Guo, W.-J. Cho, C.-S. Ha, Synthesis and characterization of novel amorphous hybrid silica materials, J. Sol-Gel Sci. Tech. 27 (2003) 333–341, https://doi.org/10.1023/A:1024077221572.
[76] M.A. Wahab, I. Kim, C.-S. Ha, Hybrid periodic mesoporous organosilica materials prepared from 1,2-bis(triethoxysilyl)ethane and (3-cyanopropyl)triethoxysilane, Microporous Mesoporous Materials 69 (2004) 19–27, https://doi.org/10.1016/j.micromeso.2004.01.001.
[77] M. Kruk, M. Jaroniec, S. Guan, S. Inagaki, Adsorption and thermogravimetric characterization of mesoporous materials with uniform organic-inorganic frameworks, J. Phys. Chem. B 105 (2001) 681–689, https://doi.org/10.1021/jp003133f.